Title
Nonlinear response of stratospheric ozone column to chlorine injections

Journal
Journal of Geophysical Research, 88(C6)

ISSN
0148-0227

Authors
Cicerone, Ralph J
Walters, Stacy
Liu, SC

Publication Date
1983-04-20

DOI
10.1029/jc088ic06p03647

JOURNAL OF GEOPHYSICAL RESEARCH, VOL. 88, NO. C6, PAGES 3647–3661, APRIL 20, 1983

Nonlinear Response of Stratospheric Ozone Column to Chlorine Injections

RALPH J. CICERONE AND STACY WALTERS

National Center for Atmospheric Research, Boulder, Colorado 80307

S. C. LIU

National Oceanic and Atmospheric Administration, Boulder, Colorado 80302

With a reasonably complete and up-to-date photochemical model of the stratosphere, we find that the calculated stratospheric ozone-column response to chlorine injections is highly nonlinear. The model calculations assume that the background inorganic (or odd) chlorine, ClX, is due to CH_3Cl and CCl_4. Additional ClX is added to the stratosphere by varying input fluxes of CCl_2F_2 and CCl_3F. The sensitivity, $\Delta O_3/\Delta ClX$, of the stratospheric O_3 column to added ClX is relatively small for Cl$X \lesssim 3$ ppb or $\Delta ClX \lesssim 2$ ppb; slight ozone increases with ClX are possible over a limited range of ClX if the formation of chlorine nitrate proceeds rapidly. This may have important implications for total ozone-column trend assessment. As ClX increases beyond 3 ppb, the stratospheric O_3 column decreases with ClX increasingly rapidly. This marked departure from the linearity calculated in past years is largely due to presently accepted faster rates of reaction of OH with HNO_3, HNO_4, HO_2, and H_2O_2. If stratospheric ClX increases to about 9 ppb due to continued usage of CCl_2F_2, CCl_3F, and CH_3CCl_3, the stratospheric O_3 column depletion is calculated to be 6.7–9.0%. Principal uncertainties in these calculations, including the rate of formation of chlorine nitrate, the products of its photolysis, and the present day mixing ratio of ClX are discussed. Calculated ozone decreases due to increased N_2O concentrations are also presented.

1. INTRODUCTION

The identification of human activities that can affect global-scale atmospheric chemistry has led to an intensification of research aimed at understanding both the natural and perturbed systems. Man's potential impact on stratospheric ozone, on the entire stratospheric photochemical system, and indirectly on climate has been recognized to involve a rich variety of coupled chemical and physical phenomena. Accordingly, efforts to understand the future impact of continued usage of chlorofluoromethanes (CFM), CH_3CCl_3, and of nitrous oxide have broadened in scope to consider the coupled effects of increasing atmospheric CO_2 and CFM concentrations [*Luther et al.*, 1977; *Haigh and Pyle*, 1979] and of stratospheric dynamics and chemistry [*Harwood and Pyle*, 1977; *Garcia and Solomon*, 1983]. Recently documented trends in atmospheric CH_4 levels [*Rasmussen and Khalil*, 1981; *Blake et al.*, 1982] have been shown [*Owens et al.*, 1982] to be capable of influencing stratospheric response to CFMs. Further, the potential interactions of simultaneous increases in N_2O and CFMs were investigated by *Logan et al.* [1978] even before the convincing documentation of an upward secular trend in N_2O concentrations appeared in print [*Weiss*, 1981]. Further, *Logan et al.* [1978] demonstrated the potential effects of combustion-produced gases on tropospheric O_3 and OH and through these OH changes, the effects on stratospheric chlorine and ozone concentrations. The more speculative but plausible increases in tropospheric ozone due to commercial aircraft operations [*Liu et al.*, 1980; *Derwent*, 1982] would necessitate a still broader view of atmospheric ozone perturbations, especially from the point of view of trend assessment in ground-based total ozone-column measurements. Simultaneous variations in CFMs, N_2O, CH_4, and tropospheric NO_x were investigated by *Wuebbles et al.* [1983].

Since 1974 when the CFM-O_3 problem was identified by *Molina and Rowland* [1974], there have been many attempts to calculate future changes in stratospheric O_3. Although more emphasis has been placed on potential decreases in the total ozone column (both in one- and two-dimensional models) the potential redistribution of ozone (large decreases at high altitudes and small changes or increases at altitudes below 30 km) is also of great scientific interest and possibly important to climate [*Crutzen*, 1974; *Ramanathan and Dickinson*, 1979]). During the 8-year period 1974–1982, the estimated sensitivity of total stratospheric ozone to CFM injections has varied [see, e.g., *NAS/NRC*, 1982] as model parameterizations and laboratory photochemistry and kinetics data improved. However, three features of the CFM-O_3 problem remained in updated calculations as originally estimated: (1) large O_3 decreases were projected near 40 km altitude; (2) as CFMs were added to the atmosphere, the total O_3 column diminished; and (3) an essentially linear response was observed between total O_3 column and the amount of added CFM, or equivalently stratospheric odd chlorine, ClX. For a representative statement on the linearity of the response, see *Miller et al.* [1978].

In this paper, we show that an updated photochemical model of the stratosphere now predicts a highly nonlinear response of total stratospheric ozone to ClX increments. It is shown further that a change in the sign of the response might occur, at least over a limited range of ClX increments. Before presenting these results in section 3 and discussing them in section 4, we describe essential features of the model in section 2.

2. THE PRESENT MODEL

Despite its obvious meteorological shortcomings, the one-dimensional eddy-diffusion/photochemical model of atmospheric chemistry has been proven to be useful especially to

Paper number 3C0075.

TABLE 1. Atmospheric Model Input Data

Altitude (km)	N (cm^{-3})	T (°K)	K_1 ($cm^2\ s^{-1}$)	K_2 ($cm^2\ s^{-1}$)
10	8.60(18)	223	9.4(4)	9.4(4)
12	6.49(18)	218	2.1(4)	2.1(4)
14	4.74(18)	217	4.6(3)	3.8(3)
16	3.46(18)	216	5.4(3)	4.3(3)
18	2.53(18)	216	6.6(3)	5.0(3)
20	1.85(18)	217	8.4(3)	6.0(3)
22	1.34(18)	218	1.0(4)	7.8(3)
24	9.76(17)	220	1.3(4)	1.0(4)
26	7.12(17)	222	1.6(4)	1.2(4)
28	5.21(17)	224	2.2(4)	1.8(4)
30	3.83(17)	226	3.1(4)	2.6(4)
32	2.82(17)	230	4.2(4)	3.4(4)
34	2.06(17)	234	5.7(4)	4.6(4)
36	1.51(17)	239	7.8(4)	6.2(4)
38	1.12(17)	245	1.1(5)	9.2(4)
40	8.31(16)	250	1.5(5)	1.3(5)
42	6.23(16)	256	2.0(5)	1.8(5)
44	4.70(16)	262	2.7(5)	2.4(5)
46	3.56(16)	266	3.7(5)	3.4(5)
48	2.74(16)	270	5.1(5)	4.7(5)
50	2.14(16)	271	7.0(5)	6.0(5)
52	1.67(16)	270	7.7(5)	7.0(5)
54	1.31(16)	267	8.4(5)	7.9(5)
56	1.03(16)	264	9.3(5)	8.9(5)
58	8.13(15)	260	1.0(6)	9.7(5)
60	6.36(15)	256	1.1(6)	1.0(6)
62	4.98(15)	250	1.2(6)	1.2(6)
64	3.92(15)	243	1.4(6)	1.4(6)
66	3.06(15)	235	1.5(6)	1.5(6)
68	2.37(15)	227	1.6(6)	1.6(6)
70	1.82(15)	220	1.7(6)	1.7(6)
72	1.38(15)	213	1.7(6)	1.7(6)
74	1.04(15)	208	1.7(6)	1.7(6)
76	7.77(14)	203	1.7(6)	1.7(6)
78	5.72(14)	199	1.9(6)	1.9(6)
80	4.16(14)	195	2.0(6)	2.0(6)

$K_1(z)$ is an altitude-dependent, eddy-diffusion coefficient that is essentially 2x the value of the 1975 Hunten coefficient [see, e.g., *Massie and Hunten*, 1981] below 30 km but larger above 30 km. $K_2(z)$ has been constructed to provide better agreement between calculated and measured vertical profiles of CH_4, N_2O, CF_2Cl_2, and $CFCl_3$. $N(z)$ is the total atmospheric number density versus altitude, and T is temperature. 8.6(18) is 8.6×10^{18}.

explore chemical sensitivities [see, e.g., *WMO*, 1982]. The present model adopts this approach wherein all vertical transport is parameterized as being proportional to concentration gradients with a common proportionality constant, $K(z)$. The spatial domain under consideration, 10–80 km, the spatial grid points, and the adopted values for $K(z)$, atmospheric temperature (fixed with time) and for atmospheric N_2 and O_2 densities are shown in Table 1. The distinction between $K_1(z)$ and $K_2(z)$ is as follows. $K_1(z)$ is essentially twice the values of the 1975 Hunten profile [*Massie and Hunten*, 1981] below 30 km but slightly greater still above 30 km. We constructed $K_2(z)$ to provide better agreement between calculated and measured values of CF_2Cl_2, $CFCl_3$, N_2O, and CH_4 than was attainable with $K_1(z)$. Note that $K_2(z)$ is not more than 28% lower than $K_1(z)$ and is closer to $K_1(z)$ at most altitudes.

Photodissociation reactions included in this model are listed in Table 2 along with the reaction products adopted for standard case calculations; nonstandard-case assumptions are discussed later and in Table 4. Table 3 lists the chemical kinetic reactions, rates, and products included explicitly in the present study's standard-case calculations; deviations from this set are discussed later and are shown in Table 4. Careful inspection of Tables 3 and 4 will show that this chemical reaction scheme includes all reactions presently believed to be significant in stratospheric ozone-layer photochemistry. Most of the photochemical and chemical kinetic data values are those selected in a recent critical review [*NASA/JPL*, 1982]. Significant departures are for k_{81} where we adopt a faster rate due to *Smith et al.* [1982] and for $\sigma(O_2)$ in the Herzberg continuum. For $\sigma(O_2)$ we have reduced those values recommended by *NASA/JPL* [1982] as suggested by *Frederick and Mentall* [1982] but our reduction is far less than that of *Herman and Mentall* [1982] or *Froidevaux and Yung* [1982]. Specifically, our cross sections (10^{-24} cm^2) are 7.1, 6.2, 5.2, 4.0, 3.4, 2.8, 1.9, and 0.8 at 207.5, 212.5, 217.5, 222.5, 227.5, 232.5, 237.5, and 242.5 nm, respectively.

Rates of photodissociation were calculated by subdividing the wavelength spectrum 175–1100 nm into 76 unequal subintervals. In the Schumann-Runge bands of O_2, the transmission formulation of *Hudson and Mahle* [1972] was employed. From 295 to 315 nm, $\Delta\lambda$ was taken as 2 nm. Photodissociation by Lyman-alpha radiation was included for CH_4, HCl, and H_2O. In all calculations, absorption by O_2 and O_3 and multiple scattering optics were included, the latter with essentially the formulation of *Luther* [1980]. Luther's method is a two-stream approximation that permits a variable number of calculations (or passes) through the scattering field. We adopted a three-pass approximation; it agreed with more accurate six-pass calculations to within 1% for J values with the largest disagreement (about 1%) near the lower boundary, 10 km. Mid-latitude equinox geometry and 30° latitude were assumed. A planar atmosphere was assumed in these calculations; corrections for a spherical atmosphere would significantly affect zenith angles over 89°. We have accounted for the variation of sunrise (sunset) time with altitude, however. For example, with our model geometry sunrise occurs at 0540 at 25 km (0600 at ground level) and sunset occurs at 1820 at 25 km (1800 at ground level).

The present model does not follow a chemical-family grouping. Instead, a mass-conservation equation is solved for each individual chemical species, and, thus, assumptions of chemical equilibrium are avoided. In particular, for steady state calculations, solutions are calculated for 32 species, and as discussed in the appendix a flux-divergence term is included in each individual species equation. These are H_2O, H_2, CH_4, CO, N_2O, CH_3Cl, CCl_4, $CFCl_3$, CF_2Cl_2, O_3, O, $N(^4S)$, NO, NO_2, NO_3, N_2O_5, HNO_3, HNO_4, H, OH, HO_2, H_2O_2, Cl, ClO, HCl, $ClONO_2$, HOCl, CH_3, CH_3O, CH_3O_2, CH_3OOH, and CH_2O. For $O(^1D)$, HCO, and ClOO photochemical equilibrium is assumed, i.e., no flux-divergence term is carried in the equations. In our time-dependent calculations, 23 species are calculated as per the appendix, and the first nine species of the 32 listed above are held fixed at specified self-consistent initial conditions.

In our steady state model, a proper 24-hour averaging is included according to the procedure of *Turco and Whitten* [1978] wherein a completely time-dependent calculation is performed and diurnal factors are determined. These factors are then employed in the steady state model, new solutions are computed, and these become new initial conditions for the time-dependent diurnal model. After iterating twice we have found that this approach yields daily averaged values from the steady state code that are within 1% of those from the nearly exact time-dependent code. In this way, potential problems with radical-radical reactions [*Johnston and Whitten*, 1975; *Turco and Whitten*, 1978] are avoided.

As noted in the appendix, two distinct types of boundary conditions are employed for the chemical species. In the steady state model at 10 km fixed-flux boundary conditions (as opposed to fixed densities) are used for N_2O, CH_3Cl, CCl_4, CF_2Cl_2, and $CFCl_3$. The exact flux values are adjusted to yield volume mixing ratios at 10 km as follows: N_2O (0.30 ppm), CH_3Cl (0.68 ppb), CCl_4 (0.125 ppb). As model parameters such as chemical reaction rates are varied, the input fluxes of these species must be readjusted to yield the stated mixing ratios. A fixed mixing ratio of 1.6 ppm is used for CH_4 at 10 km except as noted in Table 4. Assuming a constant flux for species like CH_3Cl (with appreciable tropospheric loss) is not an essential procedure; one might select a constant mixing ratio instead. Fluxes for CF_2Cl_2 and $CFCl_3$ are varied to produce variable amounts of stratospheric inorganic (or odd) chlorine, Cl*X*. Other boundary conditions for the remaining species and for time-dependent calculations have been tested carefully and are displayed in the appendix.

Certain model calculations reported below were compared with those of a second model. The latter model is essentially that of *Liu et al.* [1976] but with updated and fuller chemical reaction schemes. The two models gave excellent agreement in calculated species concentrations and in the essential nonlinear character of O_3-Cl*X* perturbations reported below. Because the Liu et al. model solves equations for grouped chemical families, it can be stated that our results do not depend on family grouping or on assumptions of chemical equilibrium, or the lack of both.

3. Results of Model Calculations

Table 4 describes fourteen different configurations of the photochemical models that we used to calculate the response of stratospheric ozone to chlorine injections. Except as noted in Table 4, the reaction rates listed in Table 3 and the photochemical data of Table 2 were employed. For example, models A-K used k_{72} (the rate of formation of $ClONO_2$) equal to one-half the faster rate listed in *NASA/JPL* [1982] while models L and M used the fast rate and model N used the *NASA/JPL* [1982] slow rate (about 25% of the fast rate). Similarly, models K, M, and N employed a new faster rate for $HCl + OH \rightarrow H_2O + Cl$, i.e., $k_{67} = 4.6 \times 10^{-12} \exp(-500/T)$ (M. J. Molina, private communication, 1982), approximately 1.2 times the value listed in Table 3. All models used $K_2(z)$ from Table 1 except for model H. Finally, an important recent adjustment to the rate of photolysis of N_2O_5, namely, a temperature-dependent photoabsorption cross section [*Yao et al.*, 1982] was incorporated into our calculations. Although the Yao et al., results are exactly those recommended in *NASA/JPL* [1982] we used the older temperature-independent cross sections [see, e.g., *Hudson and Reed*, 1979] for models A–D. Further, in models F and G we assumed that the products of N_2O_5 photolysis are $2NO_2 + O$, contrary to recent data (H. S. Johnston, private communication, 1982).

Because of the remaining uncertainties in laboratory kinetic data for k_{72} and k_{67}, it is not completely clear as to which of the models of Table 4 are to be preferred. Models A, B, C, D, F, G, H, and I are not defensible based on available data; they were employed to study sensitivities. Further, model J, while possible, is hard to defend as available evidence suggests that $ClONO_2 + h\nu \rightarrow Cl + NO_3$, not $ClO + NO_2$. Models E, K, L, M, N are most likely, but k_{72} is probably not the intermediate, standard value adopted in Table 3 and models E and K; it is either the *NASA/JPL* [1982] fast rate or the slow rate. Assuming that k_{67} is best chosen as the new, faster rate, our preferred models are M and N. Note once again that the rate, k_{72}, of formation of chlorine nitrate is four times faster in model M than in model N.

TABLE 2. Photodissociation Reactions and Products Included in the Model and References for Photoabsorption Coefficients

Photolysis	Rate	Reference
$O_2 + h\nu = O + O$	J_1	$175 < \lambda < 205$ nm: *Hudson and Mahle* [1972] $205 < \lambda < 242$ nm: see text *Hudson and Kiefer* [1975]
$O_3 + h\nu = O_2 + O$	J_2	
$O_3 + h\nu = O_2 + O(^1D)$	J_3	
$NO_2 + h\nu = NO + O$	J_4	
$N_2O + h\nu = N_2 + O(^1D)$	J_5	
$HNO_3 + h\nu = OH + NO_2$	J_6	
$H_2O_2 + h\nu = OH + OH$	J_7	
$NO_3 + h\nu = NO + O_2$	J_8	
$H_2CO + h\nu = H + HCO$	J_9	
$H_2CO + h\nu = H_2 + CO$	J_{10}	
$CF_2Cl_2 + h\nu = Cl + CF_2Cl$	J_{11}	
$CFCl_3 + h\nu = Cl + CFCl_2$	J_{12}	
$ClONO_2 + h\nu = Cl + NO_3$	J_{13}	*Marinelli and Johnston* [1982]
$HCl + h\nu = H + Cl$	J_{14}	
$HOCl + h\nu = OH + Cl$	J_{15}	
$N_2O_5 + h\nu = NO_2 + NO_3$	J_{16}	
$CH_3OOH + h\nu = OH + CH_3O$	J_{17}	
$CCl_4 + h\nu = Cl + CCl_3$	J_{18}	
$HNO_4 + h\nu = HO_2 + NO_2$	J_{19}	
$CH_3O_2 + h\nu = CH_3 + O_2$	J_{20}	*Kan et al.* [1979]
$NO + h\nu = N + O$	J_{21}	*Nicolet* [1979]
$NO_3 + h\nu = NO_2 + O$	J_{22}	
$CH_4 + h\nu = H + CH_3$	J_{23}	*Sun and Weissler* [1955]
$H_2O + h\nu = H + OH$	J_{24}	*Hudson and Kieffer* [1975]

Where no reference is shown, the critical review recommendations from *NASA/JPL* [1982] were adopted. Deviations from these standard rates and photodissociation products in certain of our calculations are noted in Table 4.

TABLE 3. Chemical Reactions, Rates, and Products Included in the Present Model

Reactions	Rate	Reference
$O + O_2 + M \rightarrow O_3 + M$		b
$O + O_3 \rightarrow O_2 + O_2$	$k_2 = 1.50E\text{-}11 \exp(-2220./T)$	a
$O + O + M \rightarrow O_2 + M$		e
$O(^1D) + N_2 \rightarrow O + N_2$	$k_4 = 1.80E\text{-}11 \exp(107./T)$	a
$O(^1D) + O_2 \rightarrow O + O_2$	$k_5 = 3.20E\text{-}11 \exp(67./T)$	a
$O(^1D) + O_3 \rightarrow O_2 + O_2$	$k_6 = 1.20E\text{-}10$	a
$O(^1D) + O_3 \rightarrow O + O + O_2$	$k_7 = 1.20E\text{-}10$	a
$O(^1D) + N_2O \rightarrow N_2 + O_2$	$k_8 = 5.10E\text{-}11$	a
$O(^1D) + N_2O \rightarrow NO + NO$	$k_9 = 6.60E\text{-}11$	a
$NO + O_3 \rightarrow NO_2 + O_2$	$k_{10} = 2.30E\text{-}12 \exp(-1450./T)$	a
$NO_2 + O \rightarrow NO + O_2$	$k_{11} = 9.30E\text{-}12$	a
$N + O_3 \rightarrow NO + O_2$	$k_{12} = 5.00E\text{-}16$	a
$N + O_2 \rightarrow NO + O$	$k_{13} = 4.40E\text{-}12 \exp(-3220./T)$	a
$NO_2 + O_3 \rightarrow NO_3 + O_2$	$k_{14} = 1.20E\text{-}13 \exp(-2450./T)$	a
$NO + NO_3 \rightarrow NO_2 + NO_2$	$k_{15} = 2.00E\text{-}11$	a
$NO + O + M \rightarrow NO_2 + M$		b
$NO_2 + NO_3 + M \rightarrow N_2O_5 + M$		b
$N_2O_5 + M \rightarrow NO_2 + NO_3 + M$	k_{18} = formula from reference f	f
$N + NO \rightarrow N_2 + O$	$k_{19} = 3.40E\text{-}11$	a
$N + NO_2 \rightarrow N_2O + O$	$k_{20} = 2.10E\text{-}11 \exp(-800./T)$	g
$O(^1D) + H_2O \rightarrow OH + OH$	$k_{21} = 2.20E\text{-}10$	a
$O(^1D) + CH_4 \rightarrow OH + CH_3$	$k_{22} = 1.40E\text{-}10$	a
$O(^1D) + CH_4 \rightarrow H_2 + H_2CO$	$k_{23} = 1.40E\text{-}11$	a
$O(^1D) + H_2 \rightarrow OH + H$	$k_{24} = 9.90E\text{-}11$	a
$H + O_3 \rightarrow OH + O_2$	$k_{25} = 1.40E\text{-}10 \exp(-470./T)$	a
$H + O_2 + M \rightarrow HO_2 + M$		b
$OH + O_3 \rightarrow HO_2 + O_2$	$k_{27} = 1.60E\text{-}12 \exp(-940./T)$	a
$HO_2 + O_3 \rightarrow OH + O_2 + O_2$	$k_{28} = 1.10E\text{-}14 \exp(-580./T)$	a*
$OH + O \rightarrow H + O_2$	$k_{29} = 2.30E\text{-}11 \exp(110./T)$	a
$HO_2 + O \rightarrow OH + O_2$	$k_{30} = 4.00E\text{-}11$	a*
$H_2O_2 + O \rightarrow OH + HO_2$	$k_{31} = 2.80E\text{-}12 \exp(-2125./T)$	a*
$OH + CH_4 \rightarrow H_2O + CH_3$	$k_{32} = 2.36E\text{-}12 \exp(-1710./T)$	a
$HO_2 + NO \rightarrow OH + NO_2$	$k_{33} = 3.50E\text{-}12 \exp(250./T)$	a*
$OH + CO \rightarrow CO_2 + H$	$k_{34} = 1.35E\text{-}13 \exp(1 + p)$	a
$OH + H_2 \rightarrow H_2O + H$	$k_{35} = 1.20E\text{-}11 \exp(-2220./T)$	g
$OH + NO_2 + M \rightarrow HNO_3 + M$		b
$OH + HNO_3 \rightarrow H_2O + NO_3$	$k_{37} = 1.52E\text{-}14 \exp(650./T)$	h
$OH + H_2O_2 \rightarrow H_2O + HO_2$	$k_{38} = 2.70E\text{-}12 \exp(-145./T)$	a*
$OH + HO_2 \rightarrow H_2O + O_2$	$k_{39} = 8.00E\text{-}11$	a*
$OH + OH \rightarrow H_2O + O$	$k_{40} = 4.50E\text{-}12 \exp(-275./T)$	a*
$OH + H_2CO \rightarrow H_2O + HCO$	$k_{41} = 1.00E\text{-}11$	a
$HO_2 + HO_2 \rightarrow H_2O_2 + O_2$		g
$OH + OH + M \rightarrow H_2O_2 + M$		b
$H + HO_2 \rightarrow H_2 + O_2$	$k_{44} = 7.40E\text{-}12$	k
$H + HO_2 \rightarrow H_2O + O$	$k_{45} = 2.22E\text{-}12$	k
$H + HO_2 \rightarrow OH + OH$	$k_{46} = 6.44E\text{-}11$	k
$H_2CO + O \rightarrow OH + HCO$	$k_{47} = 3.00E\text{-}11 \exp(-1550./T)$	a
$CH_3 + O_2 + M \rightarrow CH_3O_2 + M$		b
$CH_3O_2 + NO \rightarrow CH_3O + NO_2$	$k_{49} = 7.40E\text{-}12$	a*
$CH_3O_2 + HO_2 \rightarrow CH_3OOH + O_2$	$k_{50} = 7.70E\text{-}14 \exp(1300./T)$	a
$CH_3OOH + OH \rightarrow CH_3O_2 + H_2O$	$k_{51} = 2.10E\text{-}12 \exp(-150./T)$	a*
$CH_3O + O_2 \rightarrow H_2CO + HO_2$	$k_{52} = 9.20E\text{-}13 \exp(-2200./T)$	g
$HCO + O_2 \rightarrow CO + HO_2$	$k_{53} = 5.00E\text{-}12$	a*
$O(^1D) + CF_2Cl_2 \rightarrow ClO + CF_2Cl$	$k_{54} = 1.40E\text{-}10$	a*
$O(^1D) + CFCl_3 \rightarrow ClO + CFCl_2$	$k_{55} = 2.20E\text{-}10$	a*
$O(^1D) + CH_3Cl \rightarrow Cl$ + negligible product	$k_{56} = 1.00E\text{-}10$	estimate
$OH + CH_3Cl \rightarrow Cl$ + negligible product	$k_{57} = 1.80E\text{-}12 \exp(-1110./T)$	a
$Cl + O_3 \rightarrow ClO + O_2$	$k_{58} = 2.80E\text{-}11 \exp(-257./T)$	a
$ClO + O \rightarrow Cl + O_2$	$k_{59} = 7.70E\text{-}11 \exp(-130./T)$	a
$ClO + NO \rightarrow Cl + NO_2$	$k_{60} = 6.50E\text{-}12 \exp(280./T)$	a
$O(^1D) + HCl \rightarrow Cl + OH$	$k_{61} = 1.40E\text{-}10$	a
$Cl + CH_4 \rightarrow HCl + CH_3$	$k_{62} = 9.60E\text{-}12 \exp(-1350./T)$	a
$Cl + HO_2 \rightarrow HCl + O_2$	$k_{63} = 4.80E\text{-}11$	a*
$Cl + H_2 \rightarrow HCl + H$	$k_{64} = 3.50E\text{-}11 \exp(-2290./T)$	a*
$HCl + H \rightarrow Cl + H_2$	$k_{65} = 4.70E\text{-}11 \exp(-2340./T)$	
$Cl + H_2O_2 \rightarrow HCl + HO_2$	$k_{66} = 1.10E\text{-}11 \exp(-980./T)$	a
$OH + HCl \rightarrow Cl + H_2O$	$k_{67} = 2.80E\text{-}12 \exp(-425./T)$	a
$Cl + O_2 + M \rightarrow ClOO + M$		b
$ClOO + M \rightarrow Cl + O_2 + M$	$k_{69} = 2.70E\text{-}09 \exp(-2650./T)$	g
$HO_2 + ClO \rightarrow HOCl + O_2$	$k_{70} = 4.60E\text{-}13 \exp(710./T)$	a
$H + ClO \rightarrow OH + Cl$	$k_{71} = 3.00E\text{-}11$	estimate

TABLE 3. (*continued*)

Reactions	Rate	Reference
$ClO + NO_2 + M \rightarrow ClONO_2 + M$		c
$ClONO_2 + O \rightarrow ClO + NO + O_2$	$k_{73} = 3.00E\text{-}12 \exp(-808./T)$	a
$ClONO_2 + OH \rightarrow HOCl + NO_3$	$k_{74} = 1.20E\text{-}12 \exp(-333./T)$	a
$H_2CO + Cl \rightarrow HCl + HCO$	$k_{75} = 9.20E\text{-}11 \exp(-68./T)$	a*
$H_2 + O \rightarrow OH + H$	$k_{76} = 8.80E\text{-}12 \exp(-4200./T)$	i
$O(^1D) + CCl_4 \rightarrow ClO + CCl_3$	$k_{77} = 3.50E\text{-}10$	a*
$OH + HOCl \rightarrow ClO + H_2O$	$k_{78} = 3.00E\text{-}12 \exp(-150./T)$	a
$HO_2 + NO_2 + M \rightarrow HNO_4 + M$		b
$HNO_4 + M \rightarrow HO_2 + NO_2 + M$		j
$HNO_4 + OH \rightarrow H_2O + O_2 + NO_2$	$k_{81} = 6.00E\text{-}13 \exp(650./T)$	d

Except as specified in Table 4, these standard values were those employed in the calculations. References for these selections are as follows:

a, *NASA/JPL* [1982].

b, all three-body reaction rates are calculated from the generalized expression and species-specific data given in *NASA/JPL* [1982].

c, for k_{72}, *NASA/JPL* [1982] gives two possible rate constants, one fast and one slow. At stratospheric conditions they differ by about a factor of 4. We adopted the *NASA/JPL* [1982] fast rate divided by two as the standard rate here.

d, *Smith et al.* [1982].

e, *Campbell and Gray* [1973].

f, *Connell and Johnston* [1979].

g, *NASA/JPL* [1981].

h, *Wine et al.* [1981].

i, *Dubinsky and McKenney* [1975].

j, *Graham et al.* [1978].

k, *Sridharan et al.* [1982].

An asterisk after a reference (e.g., a*) indicates that the adopted rate constant or reaction product is within the range of that recommended by reference a.

Focusing immediately on the response of O_3 to added odd chlorine (Cl*X*), Figures 1*a* and 1*b* show the calculated steady state O_3 vertical profiles for models B, E, and M. In model B we intentionally used older rates for the reactions OH + HNO_3 (slower) and OH + HNO_4 (slower) and for N_2O_5 photolysis (faster). Increasing Cl*X* from 1.01 ppb to 8.94 ppb decreased O_3 at all altitudes in the stratosphere (see Figure 1*b*) and the total ozone column decreased 17.4% (see Table 5). In models E and M where presently accepted reaction rates and cross sections but different values for k_{72} and k_{67} were used, Figure 1*b* shows that O_3 decreased at altitudes above about 25 km and increased below about 25 km as Cl*X* increases. Table 5 lists the values of Cl*X* and of the ozone column (above 10 km) for each calculated point within each model group for these three models and the 11 others characterized in Table 4.

The nonlinearity of the calculated response of the stratospheric O_3 column to added Cl*X* is documented in Table 5. The slope of the O_3-Cl*X* curve is listed in the right-hand column of Table 5. Individual entries in that column are calculated by dividing the ozone change in that row by the amount of added

TABLE 4. Distinguishing Characteristics of Models A–N

Model	Kinetic Parameters	Temperature-Dependent σN_2O_5?	Other Characteristics
A		no	
B	$k_{37}/4$, $k_{81}/10$	no	
C	$k_{39}/2$, $k_{81}/10$	no	
D	$k_{39}/2$, $k_{81}/10$	no	fixed CH_4 flux at 10 km
E		yes	
F	$N_2O_5 + h\nu \rightarrow 2\ NO_2 + O$	yes	
G	$k_{37}/4$, $k_{39}/2$, $k_{81}/10$ and $N_2O_5 + h\nu \rightarrow 2\ NO_2 + O$	yes	
H		yes	$K_1(z)$ (see Table 1)
I	$k_{70}/10$	yes	
J	$ClONO_2 + h\nu \rightarrow ClO + NO_2$	yes	
K	$k_{67} = 4.6\ E\text{-}12 \exp(-500/T)$	yes	
L	k_{72} = NASA/JPL fast rate	yes	
M	k_{72} = NASA/JPL fast rate and $k_{67} = 4.6\ E\text{-}12 \exp(-500/T)$	yes	
N	k_{72} = NASA/JPL slow rate and $k_{67} = 4.6\ E\text{-}12 \exp(-500/T)$	yes	

Standard rates and products of kinetic and photochemical reactions are shown in Tables 3 and 2; differences from standard choices are indicated here. Standard eddy-mixing coefficient is $K_2(z)$ (see Table 1) except for model H. Methane was held at 1.60 ppm by volume at 10 km except in model D, where a fixed flux of 7.4×10^9 cm^{-2} s^{-1} was used. In models K, M, and N the rate for HCl + OH → H_2O + Cl, i.e., k_{67} is from M. J. Molina (private communication, 1982).

TABLE 5. Calculated Response of Stratospheric Ozone Column, $\int_{10}^{80} O_3\, dz$, versus inorganic (or odd) chlorine, ClX

ClX(ppb)	$\int_{10}^{80} O_3\, dz$ (10^{18} cm^{-2})	$-\Delta \int_{10}^{80} O_3\, dz$ (%).	$-\Delta_3/\Delta$ClX (%/ppb)
	Model A		
1.14	9.460		
2.52	9.450	0.10	.077
5.42	9.366	0.99	.230
9.36	9.049	4.35	.530
	Model B		
1.01	9.745		
2.37	9.538	2.12	1.56
5.21	9.012	7.52	1.79
8.94	8.049	17.40	2.19
	Model C		
0.96	9.730		
2.33	9.561	1.74	1.27
5.15	9.095	6.53	1.56
8.85	8.181	15.92	1.79
	Model D		
0.98	9.721		
2.34	9.545	1.81	1.33
5.16	9.035	7.06	1.69
8.75	7.959	18.10	2.33
	Model E		
1.16	9.666		
2.54	9.644	0.23	0.165
5.45	9.508	1.63	0.380
9.34	9.037	6.51	0.80
	Model F		
1.15	9.582		
1.84	9.579	0.03	0.045
2.53	9.570	0.12	0.09
5.44	9.470	1.17	0.27
9.36	9.089	5.15	0.63
	Model G		
0.94	9.724		
1.62	9.572	1.56	2.29
2.29	9.412	3.21	2.38
5.07	8.691	10.62	2.57
8.67	7.483	23.05	2.98
	Model H		
1.14	10.05		
1.82	10.04	0.10	0.15
2.49	10.03	0.20	0.15
4.64	9.927	1.22	0.35
7.92	9.605	4.43	0.65
	Model I		
1.16	9.672		
2.54	9.660	0.12	0.09
9.39	9.195	4.93	0.60
	Model J		
1.16	9.635		
1.84	9.616	0.20	0.29
2.53	9.590	0.47	0.34
5.43	9.444	1.98	0.46
9.39	9.126	5.28	0.64
	Model K		
1.16	9.665		
1.85	9.656	0.09	0.13
2.53	9.635	0.31	0.23
5.42	9.463	2.09	0.49
9.23	8.874	8.18	1.01
	Model L		
1.16	9.711		
1.86	9.728	−0.18	−0.26
2.56	9.737	−0.27	−0.19
3.10	9.739	−0.29	−0.15
5.51	9.674	0.38	0.08
9.48	9.200	5.26	0.63
	Model M		
1.16	9.716		
1.86	9.733	−0.17	−0.25
2.55	9.740	−0.25	−0.18
3.10	9.739	−0.24	−0.12
5.49	9.646	0.72	0.17
7.51	9.425	3.00	0.47
9.38	9.057	6.78	0.83
	Model N		
1.16	9.629		
1.84	9.601	0.29	0.43
2.52	9.565	0.66	0.49
5.37	9.338	3.02	0.72
9.12	8.767	8.95	1.12

The ClX mixing ratio (ppb) is the high altitude asymptote of the ClX vertical profile [see Figure 1 of *Cicerone*, 1981]. The lowest value of ClX in each model group (e.g., 1.14 ppb in model A) resulted from the input fluxes of CH_3Cl and CCl_4 discussed in the text and no CF_2Cl_2 or $CFCl_3$. The highest ClX value in each model group (e.g., 9.36 ppb in model A) resulted from adding input fluxes of 1.5×10^7 cm^{-2} s^{-1} for CF_2Cl_2 and 10^7 cm^{-2} s^{-1} for $CFCl_3$. Ozone changes were calculated by comparing the calculated ozone columns with zero and nonzero CF_2Cl_2 and $CFCl_3$ inputs. The last column to the right is calculated by dividing the total ozone change by the change in ClX starting from zero CF_2Cl_2 and zero $CFCl_3$. If the total-ozone response were linear the entries in the right-hand column within each model group would be equal regardless of ClX.

ClX, i.e., the value of ClX in that row of the table minus the minimum value for the model group. The lowest value of ClX in each model group resulted from fixed-flux inputs of CH_3Cl and CCl_4 and zero CF_2Cl_2 and $CFCl_3$. Highest values of ClX in each model group, e.g., 9.36 ppb in model A, resulted from full fluxes for CF_2Cl_2 and $CFCl_3$, 1.5×10^7 and 1.0×10^7 cm s^{-1}, respectively, or 484,000 and 358,000 metric tons annually. Intermediate ClX values resulted from portions of these CFM fluxes. Within each model group, fluxes of CH_3Cl, CCl_4, and N_2O were held fixed at the value that yielded the desired mixing ratios (listed above) when no CCl_2F_2 or CCl_3F was present.

If the response of total ozone to added ClX were linear the slopes in the right-hand column of Table 5 would be constant within each model group. Instead, the slopes are functions of ClX, often strong functions varying by factors of 5 or more or even changing sign in models L and M. Figure 2 shows the calculated ozone changes versus ClX for five different models. The responses are all nonlinear. Indeed, model M shows a net column ozone increase for ΔClX less than about 3 ppb. The most nearly linear responses are found for models B, C, D, and G (see Table 5), all of which models are characterized by lower (and presently unaccepted) reaction rates for OH (i.e., not the standard rates of Table 3). O_3 is reduced at all altitudes for models B, C, D, and G. For model J wherein an altered product distribution ($ClO + NO_2$) is assumed in photolysis of $ClONO_2$, the ozone response is moderately nonlinear (slope changes by about 100%) for ΔClX between 1 and 8 ppb and O_3 is reduced above 24 km but increased below 24 km when ΔClX = 8.23 ppb. Recently, *Marinelli and Johnston* [1982]

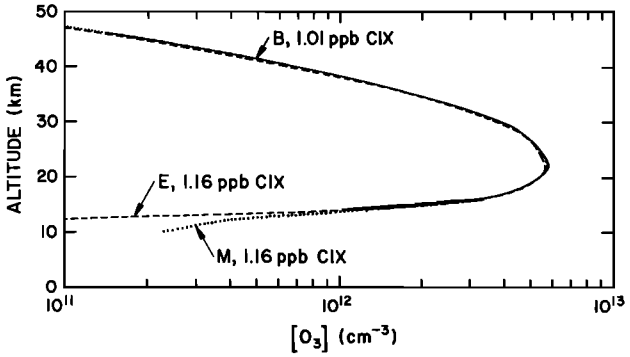

Fig. 1*a*

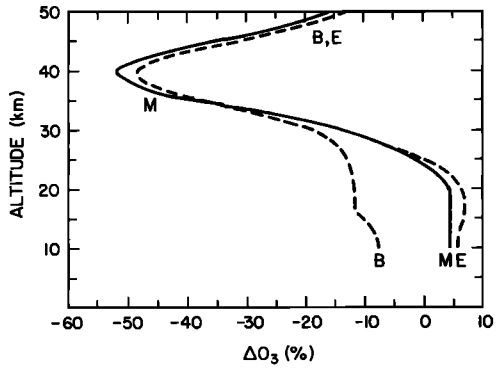

Fig. 1*b*

Fig. 1. Ozone densities (cm^{-3}) versus altitude calculated for background stratospheres, Figure 1*a* (Cl*X* due only to CH_3Cl and CCl_4 inputs) and for Cl*X*-perturbed stratospheres, Figure 1*b*. The added Cl*X* resulted from steady state input fluxes of CCl_2F_2 and CCl_3F of 1.5×10^7 and 10^7 cm^{-2} s^{-1}, respectively. In Figure 1*b*, model B, note that O_3 is decreased at all altitudes; model E, O_3 is decreased above 25 km and increased below there and in model M, O_3 is decreased above 24 km but increased below 24 km. See also Figure 3. See Table 4 for distinguishing characteristics of these models.

have presented new evidence that the principal products (over 55%) are Cl and NO_3 in chlorine nitrate photolysis.

Let us look more closely at the effects of adding chlorine to the stratosphere by focusing on two models, one (B) that is nearly linear in its response of column ozone to Cl*X* and model M which is highly nonlinear. Figures 3*a* and 3*b* show the calculated change in O_3 versus altitude for these models for three different levels of Cl*X*. The linear scale (i.e., ΔO_3 in units of 10^{11} cm^{-3}) allows one to see that the calculated nonlinear response of the stratospheric ozone column arises from the increase of ozone that appears below about 26 km. Qualitatively, the sequence of events that occur as Cl*X* is increased is clear. First, the decrease in O_3 above 30 km allows more UV light to penetrate to altitudes below 30 km, Wavelengths below 240 nm dissociate O_2, and the ozone production rates increase. Larger UV fluxes ($\lambda < 310$ nm) also lead to elevated levels of $O(^1D)$ and thus increased OH and the ratio of HCl/ClO decreases. Further, the higher concentrations of ClO (elevated both by increased Cl*X* and by the OH effect) allow more $ClONO_2$ to form, thus sequestering more NO_2. Higher ClO also increases the ratio NO_2/NO through reaction No. 60. Many other chemical feedbacks also begin, e.g., CF_2Cl_2, N_2O, etc., are photodissociated more rapidly. Also, as the shape of the O_3 profile changes, vertical fluxes of O_3 change. Accordingly, the extent of ozone healing (increases below 26 or 28 km) must depend on a number of factors.

To see more clearly how the nonlinearities arise requires more detailed analysis. We have examined ozone production and loss processes at several key altitudes. A term-by-term analysis of ozone production and loss terms at 26 km appears in Table 6 for models B and M. Recall from Table 5 that model B gave a nearly linear response and model M was highly nonlinear. Table 6 lists, for four Cl*X* levels in model B and seven Cl*X* levels in model M, the values of the terms $2J_1[O_2]$, $2k_{59}[ClO][O]$, $2k_{11}[NO_2][O]$, $2k_2[O][O_3]$, $2k_{28}[HO_2][O_3]$, $2J_{15}[HOCl]$, and $2J_{13}[ClONO_2]/9$. The latter two terms represent ozone volume destruction rates (cm^{-3} s^{-1}) due to the catalytic cycles [*Wuebbles and Chang*, 1981]

$$OH + O_3 \rightarrow HO_2 + O_2$$
$$Cl + O_3 \rightarrow ClO + O_2$$
$$HO_2 + ClO \rightarrow HOCl + O_2$$
$$HOCl + h\nu \rightarrow OH + Cl$$
$$\text{net:} \quad 2\,O_3 + h\nu \rightarrow 3\,O_2$$

and

$$Cl + O_3 \rightarrow ClO + O_2$$
$$NO + O_3 \rightarrow NO_2 + O_2$$
$$ClO + NO_2 + M \rightarrow ClONO_2 + M$$
$$ClONO_2 + h\nu \rightarrow Cl + NO_3$$
$$NO_3 + h\nu \rightarrow NO + O_2$$
$$\text{net:} \quad 2\,O_3 + 2h\nu \rightarrow 3\,O_2$$

The factor 1/9 multiplying $2J_{13}[ClONO_2]$ arises from the fact that NO_3 photolysis yields NO only 1/9 of the time and NO_2 8/9 of the time [*Magnotta and Johnston*, 1980]. The analysis of the seven terms shown in Table 6 is purely diagnostic because

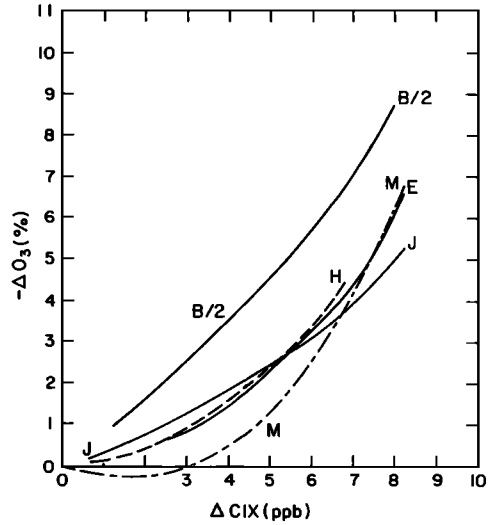

Fig. 2. Calculated percentage decreases in the vertical ozone column between 10 and 80 km for five of the models listed in Table 4, as functions of added Cl*X*. Note that model M shows an ozone increase for $\Delta ClX < 3$ ppb and that the ozone decreases shown for model B are half the computed values for convenience of display. Aside from model B, all response curves are markedly nonlinear; see also Table 5.

TABLE 6. Term-by-Term Analysis of Principal Ozone Production and Loss Processes at 26 km Altitude.

ClX(ppb)	1.16	1.86	2.55	3.10	5.49	7.51	9.38
			Model M				
$2J_1[O_2]$	6.54(5)	6.69(5)	6.87(5)	7.02(5)	7.87(5)	8.92(5)	10.33(5)
$2k_{59}[ClO][O]$	2.29(4)	3.89(4)	5.74(4)	7.34(4)	1.68(5)	2.90(5)	4.57(5)
$2k_{28}[HO_2][O_3]$	3.58(4)	3.87(4)	4.15(4)	4.37(4)	5.33(4)	5.98(4)	6.23(4)
$2J_{15}[HOCl]$	2.2 (3)	4.0 (3)	6.2 (3)	8.2 (3)	2.21(4)	4.39(4)	7.77(4)
$2k_{11}[NO_2][O]$	4.56(5)	4.43(5)	4.28(5)	4.17(5)	3.60(5)	3.04(5)	2.47(5)
$2k_2[O][O_3]$	9.21(4)	9.42(4)	9.60(4)	9.71(4)	9.94(4)	9.67(4)	8.95(4)
$2J_{13}[ClONO_2]/9$	1.2 (3)	1.9 (3)	2.6 (3)	3.2 (3)	6.2 (3)	9.3 (3)	1.26(4)
P − L	4.38(4)	4.83(4)	5.53(4)	5.94(4)	7.8 (4)	8.83(4)	8.70(4)
ClX(ppb)		1.01	2.37		5.21		8.94
			Model B				
$2J_1[O_2]$		6.56(5)	7.15(5)		8.67(5)		1.17(6)
$2k_{59}[ClO][O]$		4.13(4)	9.77(4)		2.47(5)		5.58(5)
$2k_{28}[HO_2][O_3]$		6.83(4)	7.16(4)		7.40(4)		6.68(4)
$2J_{15}[HOCl]$		7.3 (3)	1.84(4)		5.07(4)		1.23(5)
$2k_{11}[NO_2][O]$		3.79(5)	3.60(5)		3.19(5)		2.49(5)
$2k_2[O][O_3]$		9.17(4)	9.06(4)		8.54(4)		7.18(4)
$2J_{13}[ClONO_2]/9$		8.5 (2)	1.9 (3)		4.5 (3)		1.04(4)
P − L		5.99(4)	7.48(4)		8.64(4)		9.10(4)

Models B and M use the standard photochemical and kinetic data of Tables 2 and 3 except as noted in Table 4. Model B (outdated kinetic data) gave a nearly linear response of total stratospheric O_3 to added ClX while model M was highly nonlinear.

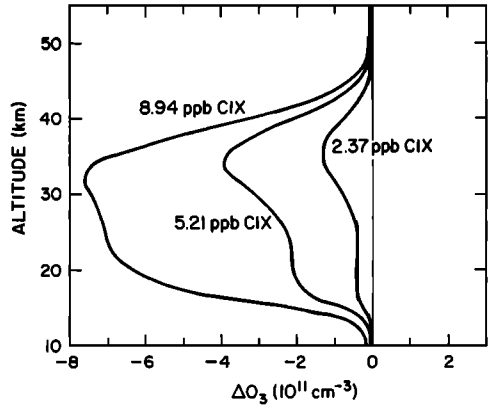

Fig. 3*a*

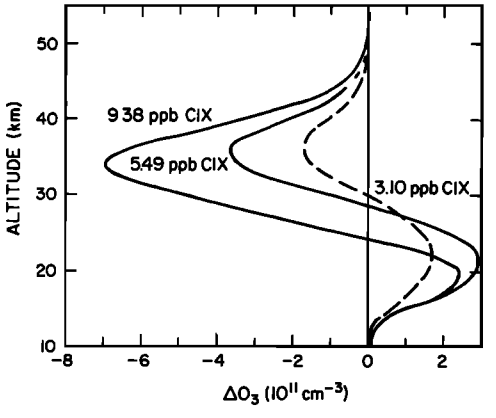

Fig. 3*b*

Fig. 3. Calculated ozone reductions (10^{11} cm^{-3}) versus altitude for several ClX mixing ratios (*a*) model B, (*b*) model M. Distinguishing features of these models are shown in Table 4.

the actual calculation did not employ chemical families; the model equations were written for individual species and rate-limiting steps for odd-oxygen destruction, for example, were not identified or calculated in the model.

Several features of Table 6 should be noted. First, the ClX-induced increase in the O_3 production rate, $2J_1[O_2]$, is pronounced at 26 km. Second, the reaction $NO_2 + O$ slows as ClX is added, largely due to the formation of additional $ClONO_2$. Also, the rates of the ozone-destroying reactions $ClO + O$ and $HOCl + h\nu$ increase with ClX but at rates that are more than simple proportionality with ClX would predict. ClO and HOCl densities increase for several reasons: (*a*) ClX increases, (*b*) NO_2 decreases as more of it is sequestered in $ClONO_2$, and (*c*) the increased penetration of UV light to 26 km leads to increased OH, thereby increasing the ClO/ClX ratio, and to increased HO_2. The increased HO_2 and ClO lead to increased HOCl and to HOCl/ClX.

This chain of events occurs in both B and M and similar net changes occur in ozone-production minus ozone-loss terms. For models B and M at 26 km, photochemical production (*P*) of O_3 exceeds losses (*L*) for all ClX values. Indeed, *P-L* increases with ClX in model B and in model M except for the last increase of ClX in model M. While this term-by-term analysis is incomplete because some less important terms have been omitted (e.g., $2k_{30}[HO_2][O]$ and $2J_8[NO_3]$ [*Johnston and Podolske*, 1978] it does indicate that an analysis of photochemical terms at a single altitude is not capable of explaining why model B differs from model M and how the nonlinear response of total column ozone originates. An analysis similar to that in Table 6 has been performed including those latter two loss terms for altitudes of 28 and 30 km. For models B and M $(P\text{-}L) > 0$ at all ClX concentrations and *P-L* increases with ClX.

A clearer view is obtained by considering ozone vertical fluxes. The need for considering the effects of transport should not be surprising because the chemical time constant, τ_c, for ozone is about 2 weeks at 30 km [*McElroy et al.*, 1974; *Prinn et*

TABLE 7. Ozone Fluxes (10^{10} cm^{-2} s^{-1}, downward) Through Four Discrete Altitudes Calculated for Various Values of Stratospheric ClX in Models B and M

Altitude (km)	1.01	2.37	5.21	8.94
Model B, ClX at 50 km (ppb)				
29	2.59	2.37	1.89	1.32
27	3.28	3.17	2.89	2.44
25	3.67	3.61	3.43	3.02
23	3.72	3.69	3.56	3.19

	1.16	1.86	2.55	3.10	5.49	7.51	9.38
Model M, ClX at 50 km (ppb)							
29	2.78	2.67	2.53	2.43	1.96	1.57	1.27
27	3.38	3.36	3.33	3.29	3.06	2.77	2.49
25	3.67	3.70	3.71	3.71	3.62	3.41	3.10
23	3.65	3.70	3.73	3.75	3.76	3.64	3.39

In model B (wherein O_3 decreases at all altitudes as ClX increases; see Figures 1*b* and 3*a*) the flux of O_3 reaching each of these altitudes from above decreases with increasing ClX. In model M (wherein the sign of the O_3 change varies with altitude between 24 and 30 km; see Figures 1*b* and 3*b*) the flux of O_3 reaching 29 and 27 km from above decreases with increasing ClX. At lower altitudes, the O_3 flux from above increases with ClX at first, then decreases as ClX increases further. This nonlinear pattern mirrors the O_3 profile changes for model M shown in Figures 1*b* and 3*b* and the total ozone versus ClX pattern of Table 5.

al., 1978] and longer below. For example, from Figure 1 and Table 6, $\tau_c = [O_3]/2J_1[O_2]$ = about 7.5×10^6 s (or about 3 months) at 25 km in an unperturbed stratosphere. These values of τ_c can be compared with an approximate time constant τ_T for vertical transport to move air between model grid points (2 km), i.e., $\tau_T \approx 2(\Delta Z)^2/K$ where K may be taken from Table 1. At 28 km $\tau_T \approx 3.6 \times 10^6$ s so $\tau_T \lesssim \tau_c$, a situation that suggests a nonlocal analysis. Table 7 presents downward ozone fluxes (10^{10} cm^{-2} s^{-1}) through the altitudes 29, 27, 25, and 23 km calculated in models B and M. Note that the downward ozone flux increases with decreasing altitude for any ClX concentration in either model(except for model M at 23 km with 1.16 ppb ClX). For comparison, *Mahlman et al.* [1980] computed a globally averaged downward flux of 5×10^{10} cm^{-2} s^{-1} at the tropopause. More relevant to the task at hand is the way these calculated fluxes change as ClX increases. In model B, the downward O_3 flux decreases at each altitude as ClX increases, just as O_3 densities behave (see Figures 1*b* and 3*b*). In model M the downward O_3 flux at 29 km decreases as ClX increases. At 27 km the downward O_3 flux decreases as ClX increases, but more slowly than at 29 km. At 25 and 23 km, the downward O_3 flux increases as ClX increases from 1.16 to 5.49 ppb, then it decreases with further increases of ClX. This pattern in the downward O_3 flux mirrors that displayed by ozone changes for model M; see Figures 1*b* and 3*b* and Table 5. As noted above, no such complicated pattern arises in Model B calculations. More generally, our present knowledge of stratospheric ozone indicates that $\tau_c < \tau_T$ above 30 km, and $\tau_c > \tau_T$ below there. Near 40 km, photochemical equilibrium is closely satisfied, and $P\text{-}L = 0$. Between about 25 and 35 km, $P\text{-}L$ exceeds zero as Table 6 exemplifies and in a one-dimensional steady state the divergence of the flux, $(d/dz)[K(z)N(z)\, df/dz = P(z) - L(z)$ is nonzero, where $f(z)$ is the ozone volume mixing ratio. This net photochemical production produces a downward flux that maintains the ozone concentrations at lower altitudes and feeds the troposphere. As chlorine is added to the stratosphere, ozone concentrations decrease above 30 km but the response below 30 km clearly depends both on photochemical processes and on transport. In our model B where the downward O_3 flux decreases with added ClX at all altitudes, there is less incoming O_3 at all altitudes below 29 km (see Table 7) and O_3 concentrations are decreased there (see Figures 1*b* and 3*a*). In our model M, O_3 is decreased above 30 km as one adds ClX and O_3 increases below there at first (see Figure 3*b*) largely due to the behavior of the downward O_3 flux (Table 7). As ClX increases further, the crossover altitude where $\Delta O_3 = 0$ moves downward. The downward movement of this crossover altitude is largely explained, at least in a one-dimensional (1-D) model, by the sign of the change in the downward O_3 flux (see Table 7) at each altitude as ClX increases.

The possibility of a strongly nonlinear response of the stratospheric zone column to added chlorine has important consequences for ozone trend detection. In Figure 4, we plot the calculated change in $\int_{10}^{80} O_3\, dz$ for the years 1970–2140. The calculated ozone column changes arise from predicted ClX values published previously by *Logan et al.* [1978] (and extrapolated here beyond A.D. 2100). In particular, we adopted case B2 of Logan et al. wherein future ClX levels are due to stated future emission rates of CCl_2F_2, CCl_3F, and CH_3CCl_3. We show two model calculations of ΔO_3, models M and N, that result from the ClX versus time curve. As shown in Table 4, a fast k_{72} (rate of formation for $ClONO_2$) is adopted in model M and a slow rate, about one-fourth as fast is adopted for k_{72} in model N. The *NASA/JPL* [1982] critical review of chemical rate constants states that both of these choices for k_{72} are presently acceptable, although in reality the true rate is either the fast rate or the slow rate, and not their average. If the fast rate applies, our model finds that ozone increases slowly until about A.D. 2010 and then ozone decreases rapidly with further increases of ClX. Table 5 shows that the total ozone decrease attained at ClX = 9.38 ppb (or ΔClX = 8.23 ppb) is 6.78% in model M. In model N, total ozone decreased by 8.95% in going to ClX = 9.12 ppb (ΔClX = 7.96 ppb).

The small, but potentially important, O_3 increases shown for model M in Table 5 and Figure 4 and for model L in Table 5 are not due to numerical inaccuracy in our model as three facts indicate. First, our numerical convergence criterion, that each variable must converge to better than 10^{-3} at each spatial grid point before terminating the iteration (see appendix), forces the

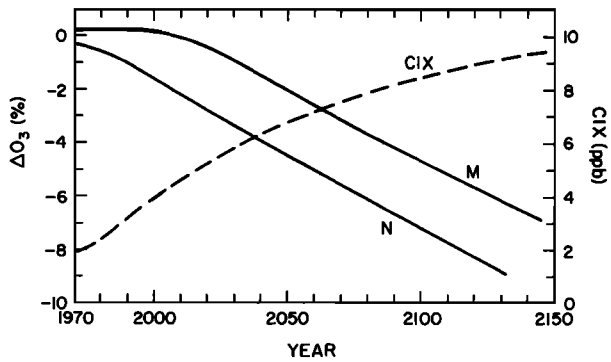

Fig. 4. Calculated column ozone ($\int_{10}^{80} O_3\, dz$) reductions expressed as a percentage of the unperturbed ozone column for models M and N. Also shown is a previously published prediction of ClX concentration [*Logan et al.*, 1978] calculated to arise due to continued usage of CCl_2F_2, CCl_3F, and CH_3CCl_3. ΔO_3 values are based on this ClX curve and the data shown in Figure 2 and Table 5. Note that model M (fast rate of formation of chlorine nitrate) column-ozone changes are positive until about A.D. 2010.

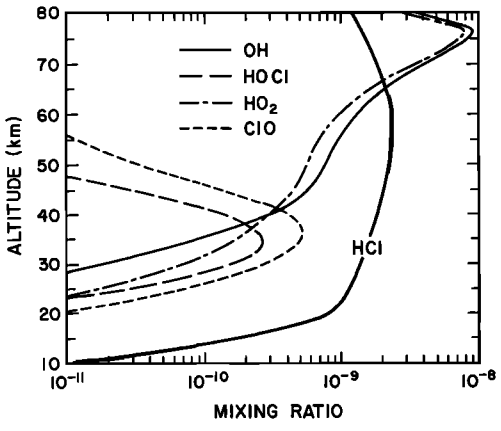

Fig. 5a. Group E rate constants.

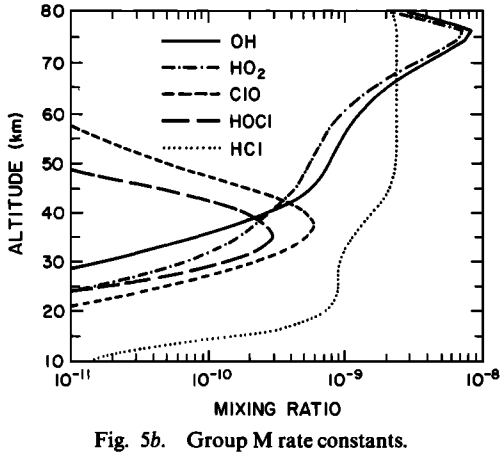

Fig. 5b. Group M rate constants.

Fig. 5. Noontime vertical profiles of mixing ratios of OH, HO_2, ClO, HOCl, and HCl calculated by our time-dependent diurnal model for (*a*) model E chemical reaction-rate data, and (*b*) model M data (see Table 4). Total inorganic chlorine, Cl*X*, mixing ratio is 2.44 ppb at 50 km in Figure 5a and 2.56 ppb in Figure 5*b*.

converged solution for the O_3 vertical profile to be at least this accurate. Even if the O_3 density at each altitude were systematically in error in the same direction (highly unlikely), the O_3 column would be in error by less than 1/1000. Table 5 shows that ozone increases of 2.5 parts in 1000 are calculated in model M, larger increases than our maximum possible numerical error. In practice, errors at one altitude should partially cancel those at another altitude, and the column integral would be more accurate. Second, we repeated certain calculations for model M but with a convergence criterion 10 times stricter (i.e., 10^{-4}), and we found an ozone column (above 10 km) identical through four decimal places to that found earlier. Both in total O_3 column and O_3 densities at individual altitudes the stricter convergence criterion led to nearly identical results through four decimal places. At only three altitudes out of 36 did the calculated O_3 density differ by as much as one unit in the fourth decimal place. Finally, as was mentioned earlier, we found similar nonlinearities in the O_3 response to Cl*X* with the chemical family approach model of *Liu et al.* [1976].

Vertical profiles of several key gas concentrations are shown in Figures 5 and 6. These profiles were calculated through the fully time-dependent model described in section 2 and the appendix. Figure 5*a* shows noontime concentrations of OH, HO_2, ClO, HOCl, and HCl versus altitude calculated with the standard photochemical data specified in Tables 2 and 3 (i.e., model E of Table 4) with Cl*X* = 2.44 ppb at 50 km. Figure 5*b* shows noontime concentrations of these species calculated with the photochemical data specified by model M of Table 4 and 2.56 ppb Cl*X*. Compare the values for the Cl-containing species: relative to Figure 3*a*, the ClO concentrations in Figure 3*b* are 0.73, 0.82, 1.10, and 1.15 at 26, 30, 40, and 44 km, respectively, when Cl*X* values are normalized to 2.56 ppb. Corresponding relative concentrations for HOCl are 0.77, 0.87, 1.09, and 1.14. For HCl they are 0.67, 0.68, 0.91, and 0.95. The high-altitude increases in ClO are clearly due to the higher value of k_{67} used in model M. An interesting feature of Figure 5*b* is the local minimum in HCl near 30 km. It results from use of the NASA/JPL fast rate for k_{72} and the new, faster value for k_{67} in model M. Such a minimum has been observed in total acidic chlorine measurements of *Lazrus et al.* [1977]. When one adds calculated HCl and HOCl values one finds a much less pronounced, gentle local minimum just below 30 km. Although contributions to stratospheric Cl*X* from CH_3CCl_3, $C_2F_3Cl_3$, and several other minor species are neglected in these diurnal calculations, the Cl*X* value (2.56 ppb) for which these calculations apply is close to what is calculated for 1982 when all known sources are included [see e.g., *Wuebbles et al.*, 1983]. In the present calculation this was accomplished by adjusting the lower boundary fluxes of CF_2Cl_2 and $CFCl_3$.

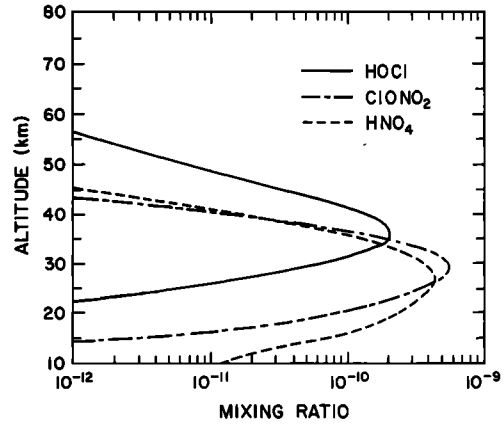

Fig. 6a. Group E rate constants.

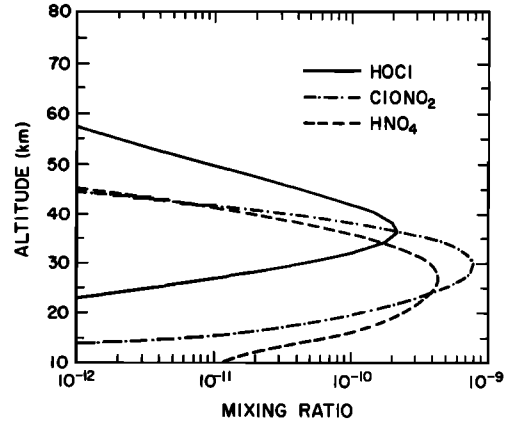

Fig. 6b. Group M rate constants.

Fig. 6*a*. Calculated vertical profiles of HOCl, $ClONO_2$, and HNO_4 for time of ground-level sunset for (*a*) model E chemical reaction-rate data and (*b*) model M data. Total inorganic chlorine, Cl*X*, mixing ratio is 2.44 ppb in Figure 6*a* and 2.55 ppb at 50 km in Figure 6*b*.

Figures 6*a* and 6*b* show calculated vertical profiles of HOCl, $ClONO_2$, and HNO_4 for time of ground sunset, Figure 6*a* for model E and Figure 6*b* for model M. In the calculation, $ClONO_2$ increases further to 0.86 ppb at 30 km by time 1830. These profiles are displayed because as is apparent in Table 5, the stratospheric ozone response is sensitive to the differences in chemical rate constants between model E and M as are the profiles of these species, and none of the species HOCl, $ClONO_2$, and HNO_4 has been measured or positively detected in the stratosphere at this writing.

Calculations have also been performed to simulate the effects of increasing atmospheric N_2O concentrations. In these calculations the input flux of N_2O was increased above the value needed to sustain a 300 ppb mixing ratio at 10 km. With all standard rate constants except for the new, faster k_{67} (i.e., model K) increasing the N_2O input flux by 50% led to a 5.27% total ozone decrease. With k_{72} twice as fast (i.e., model M) total ozone decreased 5.56% and with the slow rate of $ClONO_2$ formation (i.e., model N) total ozone decreased 5.04%. These calculations with 150% normal N_2O flux inputs lead to N_2O mixing ratios of 440 $\pm$ 3 ppb at 10 km. The calculations took fixed fluxes of CH_3Cl, CCl_4, CF_2Cl_2, and $CFCl_3$; Cl*X* began at about 2.52 ppb and dropped to about 2.42 ppb as N_2O increased. When the Cl*X* background was raised to 5.3 ppb and the N_2O flux subsequently increased by 50%, the added N_2O led to total ozone decreases of 3.05, 3.38, and 2.85% for models K, M, and N rate constants, respectively. Further calculations were performed to examine the linearity of the O_3 response to added N_2O. The input flux of N_2O was varied between the value needed to produce 300 ppb N_2O at 10 km in an unperturbed atmosphere to flux values 1.2, 1.5, and 2.2 times larger. With near-present Cl*X* background, i.e., 2.52 ppb, a slight nonlinearity appeared in the sense that the percentage ozone loss per ppb of added N_2O decreased as N_2O levels increased. At higher, presumably future levels of stratospheric Cl*X* (5.3 ppb), the nonlinearity switched sense (i.e., the O_3 loss per unit of added N_2O increased as N_2O increased).

The corresponding increased production of stratospheric NO and downward flux of odd nitrogen into the troposphere would tend to increase the tropospheric odd nitrogen. This may in turn increase tropospheric ozone.

4. Discussion and Conclusion

In this report we have shown that a distinctly nonlinear response of the stratospheric ozone column to chlorine injections is likely, or at least, this is the response predicted by our updated 1-D photochemical models. Specifically, Table 5 and Figure 2 showed that the sensitivity of total stratospheric ozone to added Cl*X*, $\Delta O_3/\Delta ClX$, is a strong function of Cl*X*, especially in the range of $1 < ClX < 4$ ppb, or $0 < \Delta ClX < 3$ ppb, where ΔClX is the Cl*X* not attributable to CH_3Cl and CCl_4. The only model calculations that showed weak or moderate nonlinearities were those that employed out-of-date rate constants for OH + HNO_3, OH + HNO_4 and OH + HO_2 or which assumed that $ClONO_2 + h\nu \rightarrow ClO + NO_2$, products not deduced in the *NASA/JPL* [1982] critical review. Given that the present Cl*X* mixing ratio (at 50 km) is now approximately 2.5 ppb (i.e., $\Delta ClX = 1.4$ or 1.5 ppb) and that $ClX = 4$ ppb (or ΔClX about = 3 ppb) is not predicted to be attained until A.D. 1995 or 2000 [*Logan et al.*, 1978; *Cicerone*, 1981], the problem of ozone trend assessment takes on a new complexity. If our calculations are accurate (see caveats below), then CFM-induced stratospheric ozone depletions of order 1% will not materialize until after A.D. 2000 when Cl*X* reaches 5 ppb or more. This latter figure comes from Table 5, models K, L, M, N, the models with presently most credible rate constants for chemical reactions. Further, as is shown in Figure 2 and Table 5, $\Delta O_3/\Delta ClX$ becomes very strongly negative for $ClX > 5$ ppb so that the rate of ozone decrease in the early 21st century could accelerate greatly. Eventual ozone column reductions due to continued release of CCl_2F_2 and CCl_3F are estimated to lie between 6.8 and 9.0% assuming a new, faster rate for OH + $HCl \rightarrow H_2O$ + Cl from M. J. Molina (private communication, 1982).

The nonlinearities evident in our results arose from an essentially controlled numerical experiment in which (1) a fixed CH_4 mixing ratio was assumed at 10 km, (2) fixed fluxes of N_2O, CH_3Cl, and CCl_4 were input at 10 km, and (3) stratospheric CO_2 and temperature were held constant. In reality, all of these factors appear to be varying; see discussion and references in section 1. Further, and very important for ground-based total ozone-column trend assessment, secular trends in tropospheric ozone are possible [see, e.g., *Liu et al.*, 1980]. A 10% change in tropospheric O_3 is about a 1% change in total ozone. The present calculations do predict large future decreases in O_3 concentrations near 40 km altitude, however, as did previous calculations.

The possibility of small stratospheric ozone-column increases cannot be eliminated. Indeed our calculations (models L and M) found this kind of result for $ClX < 3$ or 4 ppb when the rate of formation, k_{72}, of $ClONO_2$ (chlorine nitrate) was set equal to the faster of the two rates in *NASA/JPL* [1982]. With the slower rate for k_{72}, i.e., one-fourth the fast rate, no ozone increases were calculated nor were they when an intermediate rate (standard rate in Table 3) was assumed. Accordingly, it appears very important to (1) settle the issue of possible isomer formation in ClO + NO_2 + M $\rightarrow$ products and to determine the rate of formation of $ClONO_2$ at stratospheric pressures and temperatures, and (2) obtain quantitative measurements of stratospheric $ClONO_2$. Many other photochemical processes, e.g., the products of HNO_4 photodissociation need further investigations.

Our results do not depend on model assumptions such as chemical family groupings or on the exact choice of $K(z)$, the eddy-diffusion coefficient. More rigorous calculations with models that embody stratospheric dynamical meteorology are clearly needed, however. Also, while it is well known that the efficiency of ozone destruction by chlorine atoms is an increasing function of altitude [*Cicerone et al.*, 1974; *Wuebbles*, 1983] and that the stratosphere of the future will receive Cl atoms from an increasingly wide spectrum of chlorocarbons and chlorofluorocarbons, our present results will not be very sensitive to changes in this input-species spectrum. Further, our small adjustment to O_2 cross sections in the Herzberg continuum (see section 2) did not affect the nonlinear character of the O_3 response to Cl*X*. If present-day stratospheric Cl*X* concentrations greatly exceed the commonly believed 2.5 ppb the total ozone response to added Cl*X* could differ greatly from that shown in Figure 4 because of the strong dependence of $\Delta O_3/\Delta ClX$ on Cl*X* shown in Figure 2 and Table 5.

Finally, our calculated loss of total stratospheric O_3 due to 50% increases in upward N_2O fluxes from the troposphere are about 5% when background Cl*X* is near presently assumed values (2.5 ppb) and near 3% if Cl*X* grows to 5.3 ppb. Small nonlinearities were observed in the ozone response to increases in N_2O levels.

APPENDIX. NUMERICAL METHODS

The analytic, one-dimensional, steady state system of continuity equations for gas-phase atmospheric trace constituents is

$$\frac{d\bar{\Phi}}{dz} = \bar{Q}(z, \bar{f}) \tag{1a}$$

$$\bar{\Phi} = -KN \frac{d\bar{f}}{dz} \tag{1b}$$

$$\bar{Q}(z, \bar{f}) = \bar{P}(z, \bar{f}) - \bar{L}(z, \bar{f}) \tag{1c}$$

where

$\bar{f} = \{f_1, \cdots, f_k\}^T$;
$\bar{f}(z)$ trace species mixing ratio vector (length k for k species);
$\bar{\Phi}(z)$ flux vector;
$K(z)$ eddy diffusion scalar;
$N(z)$ total atmospheric density scalar;
$\bar{Q}(z, \bar{f})$ vector of photochemical forcing;
$\bar{P}(z, \bar{f})$ vector of photochemical production;
$\bar{L}(z, \bar{f})$ vector of photochemical loss;
z vertical spatial coordinate ($z_l < z < z_u$).

with attendant boundary conditions for each species in one of the following forms:

$$-KN \left.\frac{df_i}{dz}\right|_{z_B} = g_i(z_B, \bar{f}(z_B)) \tag{1d}$$

$$g_i(z_B, \bar{f}(z_B)) = 0 \tag{1e}$$

where

$$z_B = z_l \qquad z_u$$

Condition (1e) for species i must explicitly include f_i. We solve system (1) in a two-phase process. First, the self adjoint flux-divergence term is replaced with a standard, centered finite difference approximation:

$$\left.\frac{d}{dz}\left(KN \frac{d\bar{f}}{dz}\right)\right|_{z_j} = \frac{(KN)_{j+1/2}}{\frac{1}{2}\Delta z_{j+1}(\Delta z_j + \Delta z_{j+1})} \times \bar{f}_{j+1} - \left[\frac{(KN)_{j+1/2}}{\frac{1}{2}\Delta z_{j+1}(\Delta z_j + \Delta z_{j+1})} + \frac{(KN)_{j-1/2}}{\frac{1}{2}\Delta z_j(\Delta z_j + \Delta z_{j+1})}\right] \times \bar{f}_j + \frac{(KN)_{j-1/2}}{\frac{1}{2}\Delta z_j(\Delta z_j + \Delta z_{j+1})} \times \bar{f}_{j-1} \tag{2}$$

for $j = 0, 1, \cdots, J$ where $\bar{f}_j$ = discrete solution vector at $z_j (j = 0, J)$, $\Delta z_j = z_j - z_{j-1}$ $(j = 1, J)$, $(KN)_{j+1/2} = KN|z_j + \frac{1}{2}\Delta z_{j+1}$, $(KN)_{j-1/2} = KN|z_j - \frac{1}{2}\Delta z_j$.

Approximation (2) is second order (first order) accurate on a uniform, (nonuniform) spatial grid, respectively. Flux boundary conditions, type (1d), are transformed via

$$KN \left.\frac{d\tilde{f}_i}{dz}\right|_{z_B} = \frac{1}{2}\left\{KN \left.\frac{d\tilde{f}_i}{dz}\right|_{j_B+1/2} + KN \left.\frac{d\tilde{f}_i}{dz}\right|_{j_B-1/2}\right\} = \frac{1}{2}\left[KN\Big|_{j_B+1/2} \times \frac{\tilde{f}_{i,j_B+1} - \tilde{f}_{i,j_B}}{\Delta z_B} + KN\Big|_{j_B-1/2} \times \frac{\tilde{f}_{i,j_B} - \tilde{f}_{i,j_B-1}}{\Delta z_B}\right] \tag{3}$$

where $j_B = 0; J$ and $\Delta z_B = \Delta z_1; \Delta z_J$.

Analogs (2) and (3) are combined to yield a nonlinear system of algebraic equations for the solution vector $\bar{\tilde{f}}$. This system can be written as

$$\bar{F}(\bar{\tilde{f}}) = T \times \bar{\tilde{f}} + \bar{G}(\bar{\tilde{f}}) = 0 \tag{4}$$

where $\bar{\tilde{f}}$ = discrete solution vector, $\bar{F}$ = vector of nonlinear equations, $\bar{G}$ = vector of discrete photochemistry forcing, $\bar{T}$ = matrix containing discrete representation of the flux divergence operator with boundary conditions.

All vectors in (4) contain $k \times (J + 1)$ components and are organized in the following manner:

$$\bar{\tilde{f}} = \{\bar{\tilde{f}}_1, \cdots, \bar{\tilde{f}}_J\}^T$$
$$\bar{\tilde{f}}_j = \{\tilde{f}_{1,j}, \cdots, \tilde{f}_{k,j}\}^T$$

In this representation each subvector $\bar{\tilde{f}}$ represents a discrete approximation to the k analytic-solution variables at altitude z_j. For convenience, in photodissociation calculations the spatial grid is mapped from top down (i.e., $z_0 = z_u$; $z_J = z_l$). The flux boundary-condition approximation, although nonstandard, is designed to force numerical conservation of the discrete equations. When the continuity equation for a compound with flux boundary conditions is numerically integrated via the trapezoidal rule, the discrete solution will give exact numerical conservation.

Completing the solution process, system (4) is iterated via a modified Newton-Raphson scheme until acceptable convergence. A relative error criterion is applied, in a max-norm sense, to the solution vector $\bar{\tilde{f}}$ in that the Newton-Raphson stepsize is constrained to be less than a given epsilon of the current discrete approximation. Additionally, $\bar{F}$ must be reduced over the entire iterative process. In our simulations we use an epsilon equal to 10^{-3}. As one test of overall accuracy, we have repeated certain calculations with $\varepsilon = 10^{-4}$ as discussed in the text. To enhance efficiency, the Jacobian matrix in the Newton-Raphson scheme is updated only when internal checks signal convergence difficulty. Every effort has been taken to vectorize the main program for operation on the CRAY 1A. Furthermore, essential subroutines to decompose the banded Jacobian and solve for the iteration step are encoded in near optimal CRAY assembly code. This has resulted in worst-case chemical simulations requiring at most one CPU second on the CRAY 1A.

In our steady state simulations we solve for 32 discrete mixing ratios at 36 spatial grid points, thereby yielding a vector system (4) of length 1152.

The time-dependent simulation exactly parallels the development of the steady state case. All spatial operator approximations in the analytic equation and boundary conditions are identical. However, the analogous system to equation (4) now represents the following system of ordinary differential equations:

$$\bar{N} \times \frac{d\bar{\tilde{f}}(t)}{dt} = \bar{F}(\bar{\tilde{f}}) = T(t) \times \bar{\tilde{f}}(t) + \bar{G}(t, \bar{\tilde{f}}) \tag{5}$$

All vectors and matrices are as defined in equation (4) with additional dependence on the temporal variable t. Furthermore, $\bar{N}$ is a block diagonal matrix of order $J + 1$ of total atmospheric density. Each diagonal block matrix is a diagonal matrix of order k wherein each entry is the total atmospheric density at altitude z_j.

We solve system (5) by applying the second-order exponential fitting scheme of *Liniger and Willoughby* [1970] at a fixed partition of a diurnal cycle. In our adaption of the exponential fitting, we determine the basic coefficients by fitting

TABLE 8. Boundary Conditions for Each of the 32 Species Calculated in the Steady State, 24-hour Averaged Model

Species	Upper Boundary Conditions	Lower Boundary Conditions
H_2O	flux = $J_{24}[H_2O]H$	MR (3.0 ppm)
HCl	flux = J_{14}[HCl]H	[HCl] = 0.9925 × OCF/v
H_2	MR(1.76 ppm)	MR(0.5 ppm)
CH_4	flux = $J_{23}[CH_4][H]$	MR(1.60 ppm)
CO	MR(1 ppm)	MR(100 ppb)
N_2O	flux = $J_5[N_2O][H]$	flux ≈ 1.4×10^9 adjustable, see text
CH_3Cl	flux = $J_{23}[CH_3Cl]H$	flux ≈ 10^7 adjustable, see text
CCl_4	flux = $J_{18}[CCl_4][H]$	flux ≈ 1.3×10^6 adjustable, see text
CCl_3F	flux = $J_{12}[CCl_3F]H$	$0 \leq$ flux $\leq 10^7$, see text
CCl_2F_2	flux = $J_{11}[CCl_2F_2]H$	$0 \leq$ flux $\leq 1.5 \times 10^7$, see text
H_2O_2	PCE	PCE
O_3	flux = 1.4×10^{10}	flux = $-[O_3]/v$
O	flux = -9.1×10^{10}	flux = $-[O]/v$
N, NO, NO_2	flux = 0	flux = $-[x]/v$, x = N, NO, NO_2
NO_3, N_2O_5	flux = 0	flux = $-[Y]/v$, $Y = NO_3$, N_2O_5
HNO_3, HNO_4	flux = 0	flux = $-[Z]/v$, $Z = HNO_3$, HNO_4
H, OH, HO_2	PCE	PCE
Cl	flux = $-J_{14}$[HCl][H]	flux = 7.5×10^{-3}OCF([X]/[ClO_x]), iterative
ClO, HOCl, $ClONO_2$	flux = 0	flux = 7.5×10^{-3}OCF([X]/[ClO_x]), iterative, X = Cl, ClO, HOCl, $ClONO_2$
CH_3, CH_3O, CH_3O_2	PCE	PCE
CH_3OOH, CH_2O	PCE	PCE

Fluxes are in units of molecules/cm^2/s and are positive upward. v = 0.3 cm/s. MR means fixed mixing ratio. OCF, the organic chlorine flux, = $[2\phi_{CCl_2F_2} + 3\phi_{CCl_3F} + 4\phi_{CCl_4} + \phi_{CH_3Cl}]$ where ϕ is the upward flux at the lower boundary. ClO_x = Cl + ClO + HOCl + $ClONO_2$. H is the scale height for each individual species at the upper boundary, 80 km. PCE means photochemical equilibrium.

to the real points −2, −4. The resultant system of nonlinear equations is solved, as in the steady state case, via a modified Newton-Raphson technique at each temporal grid point.

Convergence is determined in exactly the same manner as the steady state algorithm. Specifically, the convergence parameter epsilon is 10^{-3}. In the diurnal simulations, we solve for 23

TABLE 9. Boundary Conditions for Each of the 23 Species Calculated in the Time-Dependent Diurnal Model.

Species	Upper Boundary Conditions		Lower Boundary Conditions	
	Day	Night	Day	Night
HCl	flux = J_{14}[HCl][H]	flux = 0	[HCl] from steady state model with same ClX	same as daytime [HCl]
H_2O_2	PCE	PCE	PCE	PCE
O_3	flux = 0	flux = $f(t)$, see appendix text	flux = $[O_3]v$	flux = $-[O_3]/v$
O	flux = $g(t)$, see appendix text	flux = $h(t)$, see appendix text	flux = $-[O]/v$	flux = $-[O]/v$
N, NO, NO_2	flux = 0	flux = 0	flux = $-[x]/v$, x = N, NO, NO_2	same equation as day
NO_3, N_2O_5	flux = 0	flux = 0	flux = $-[Y]/v$, $Y = NO_3$, N_2O_5	same equation as day
HNO_3, HNO_4	flux = 0	flux = 0	flux = $-[Z]/v$, $Z = HNO_3$, HNO_4	same equation as day
H, HO, HO_2	PCE	PCE	PCE	PCE
Cl	flux = $-J_{14}$[HCl][H]	flux = 0	flux = [Cl](ClO_x flux from corresponding steady state model with same ClX)/[ClO_x], iterative	same equation as day
ClO, HOCl, $ClONO_2$	flux = 0	flux = 0	flux = [X](ClO_x flux from corresponding steady state model with same ClX)/[ClO_x], iterative	same equation as day
CH_3, CH_3O, CH_3O_2	PCE	PCE	PCE	PCE
CH_3OOH, CH_2O	PCE	PCE	PCE	PCE

All symbols are the same as listed in Table 8.

discrete variables at 36 spatial grid points. The diurnal temporal cycle is partitioned into 35 nonuniform temporal steps ranging from 2 min to 2 hours. A typical 12 day simulation of this system takes roughly 70 CPU seconds on the CRAY 1A.

Boundary conditions for the 32 species calculated in the steady state, 24-hour averaged model are shown in Table 8, and for the 23 species calculated in the time-dependent diurnal model are shown in Table 9. In both programs the species HCO, $O(^1D)$, and ClOO are calculated from photochemical equilibrium equations at all spatial grid points and times. In the time-dependent calculation, the total downward flux of O_x, (O and O_3) at the upper boundary (80 km) integrated over a 24-hour period equals 1.05×10^{11} cm^{-2} s^{-1} as in the 24-hour averaged model (see Table 8). In the time-dependent calculation, it is apportioned as follows: the O_x flux is a sinusoidal function with period 24 hours. In the day, all the flux is in O atoms; the function $g(t)$ peaks at noon. At sunset the O atom flux decreases with an e folding time of 4.5 hours; $h(t)$ = [flux of O_x] exp [$-(t - 1800$ h)/4.5]. The O_3 flux is zero at 1800 hours and rises with an e folding time of 4.5 hours. Its flux = $f(t)$ = [O_x flux] $\times$ [$1 - \exp(-(t - 1800$ h)/4.5)].

Acknowledgment. R. Cicerone thanks H. S. Johnston for serving as editor for this paper. The National Center for Atmospheric Research is sponsored by the National Science Foundation.

REFERENCES

Blake, D. R., E. D. Mayer, S. C. Tyler, Y. Makide, D. C. Montague, and F. S. Rowland, Global increase in atmospheric methane concentrations between 1978 and 1980, *Geophys. Res. Lett.*, *9*, 477, 1982.

Campbell, I. M., and C. N. Gray, Rate constants for $O(^3p)$ recombination and association with $N(^4S)$, *Chem. Phys. Lett.*, *18*, 607–609, 1973.

Cicerone, R. J., R. S. Stolarski, and S. Walters, Stratospheric ozone destruction by man-made chlorofluoromethanes, *Science*, *185*, 1165–1167, 1974.

Cicerone, R. J., Halogens in the atmosphere, *Rev. Geophys. Space Phys.*, *19*, 123–139, 1981.

Connell, P. S., and H. S. Johnston, The thermal dissociation of N_2O_5 in N_2, *Geophys. Res. Lett.*, *6*, 553–556, 1979.

Crutzen, P. J., Estimates of possible future ozone reductions from continued use of fluorochloromethanes (CF_2Cl_2, $CFCl_3$), *Geophys. Res. Lett.*, *1*, 205–208, 1974.

Derwent, R. G., Two-dimensional model studies of the impact of aircraft exhaust emissions on tropospheric ozone, *Atmos. Environ.*, *16*, 1997–2007, 1982.

Dubinsky, R. N., and D. J. McKenney, Determination of the rate constant of $O + H_2 \rightarrow OH + H$ reaction using atomic oxygen resonance fluorescence and the air afterglow techniques, *Can. J. Chem.*, *53*, 3531–3541, 1975.

Frederick, J. E., and J. E. Mentall, Solar irradiance in the stratosphere: Implications for the herzberg continuum absorption of O_2, *Geophys. Res. Lett.*, *9*, 461–464, 1982.

Froideveaux, L., and Y. L. Yung, Radiation and chemistry in the stratosphere: Sensitivity to O_2 absorption cross sections in the Herzberg continuum, *Geophys. Res. Lett.*, *9*, 854–857, 1982.

Garcia, R., and S. Solomon, A numerical model of the zonally averaged dynamical and chemical structure of the middle atmosphere, *J. Geophys. Res.*, *88*, 1379, 1983.

Graham, R. A., A. M. Winer, and J. N. Pitts, Jr., Pressure and temperature dependence of the unimolecular decomposition of HO_2NO_2, *J. Chem. Phys.*, *68*, 4505–4510, 1978.

Haigh, J. D., and J. A. Pyle, A Two-dimensional calculation including atmospheric carbon dioxide and stratospheric ozone, *Nature*, *279*, 222–224, 1979.

Harwood, R. S., and J. A. Pyle, Studies of the ozone budget using a zonal mean circulation model and linearlized photochemistry, *Q. J. R. Meteorol. Soc.*, *103*, 319–343, 1977.

Herman, J. R., and J. E. Mentall, The direct and scattered solar flux within the stratosphere, *J. Geophys. Res.*, *87*, 1319–1330, 1982.

Hudson, R. D., and L. J. Kiefer, Absorption cross sections of stratospheric molecules, in *The Natural Stratosphere of 1974*, *CIAP Monogr.* vol. 1, pp. 5–156, *DOT-TST-75-51*, U.S. Department of Transportation, Washington, D.C., 1975.

Hudson, R. D., and J. H. Mahle, Photodissociation rates of molecular oxygen in the mesosphere and lower thermosphere, *J. Geophys. Res.*, *77*, 2402, 1972.

Hudson, R. D., and E. I. Reed (Eds.), *The Stratosphere: Present and Future*, *NASA Ref. Publ. 1049*, 1979.

Johnston, H. S., and G. Whitten, Chemical reactions in the atmosphere as studies by the method of instantaneous rates, *Int. J. Chem. Kinet.*, *7*, 1–26, 1975.

Kan, C. S., R. D. McQuigg, M. R. Whitbeck, and J. G. Calvert, Kinetic flash spectroscopic study of the CH_3O_2-CH_3O_2 and CH_3O_2-SO_2 reactions, *Int. J. Chem. Kinet.*, *11*, 921–933, 1979.

Lazrus, A. L., B. W. Gandrud, J. Greenberg, J. Bonelli, E. Mroz, and W. A. Sedlacek, Midlatitude seasonal measurements of stratospheric acidic chlorine vapor, *Geophys. Res. Lett.*, *4*, 587–589, 1977.

Liniger, W., and R. Willoughby, Efficient integration methods for stiff systems of ordinary differential equations, *SIAM J. Numer. Anal.*, *7*, 47–66, 1970.

Liu, S. C., T. M. Donahue, R. J. Cicerone, and W. L. Chameides, Effect of water vapor on the destruction of ozone in the stratosphere perturbed by Cl*X* or NO_x pollutants, *J. Geophys. Res.*, *81*, 3111–3118, 1976.

Liu, S. C., D. Kley, M. McFarland, J. D. Mahlman, and H. Levy II, On the origin of tropospheric ozone, *J. Geophys. Res.*, *85*, 7546–7552, 1980.

Logan, J. A., M. J. Prather, S. C. Wofsy, and M. B. McElroy, Atmospheric chemistry: Response of human influence, *Phil. Trans. R. Soc. London*, *290*, 187–234, 1978.

Luther, F., Photochemical modeling: A numerically fast scheme for treating multiple scattering, paper presented at the International Radiation Symposium, Ins. Assoc. of Atmos. Phys., World Meteorol. Organ. and Am. Meteorol. Soc., Ft. Collins, Colorado, Aug. 11–16, 1980.

Luther, F. M., D. J. Wuebbles, and J. S. Chang, Temperature feedback in a stratospheric model, *J. Geophys. Res.*, *82*, 4935–4942, 1977.

Magnotta, F., and H. S. Johnston, Absolute photodissociation quantum yields for the NO_3 free radical, *Geophys. Res. Lett.*, *7*, 769–772, 1980.

Mahlman, J. D., H. Levy, and W. J. Moxim, Three-dimensional tracer structure and behavior as simulated in two ozone precursor experiments, *J. Atmos. Sci.*, *37*, 655–685, 1980.

Marinelli, W. J., and H. S. Johnston, Quantum yield for NO_3 production from photolysis of $ClONO_2$, *Chem. Phys. Lett.*, *93*, 127–132, 1982.

Massie, S. T., and D. M. Hunten, Stratospheric eddy diffusion coefficients from tracer data, *J. Geophys. Res.*, *86*, 9859, 1981.

McElroy, M. B., S. C. Wofsy, J. E. Penner, and J. C. McConnell, Atmospheric ozone: possible impact of stratospheric aviation, *J. Atmos. Sci.*, *31*, 287–303, 1974.

Miller, C., P. Meakin, R. G. E. Franks, and J. P. Jesson, The fluorocarbon-ozone theory, 5, One-dimensional modeling of the atmosphere: The base case, *Atmos. Environ.*, *12*, 2481–2500, 1978.

Molina, M. J., and F. S. Rowland, Stratospheric sink for chloroflurometh anes: Chlorine-atom catalysed destruction of ozone, *Nature*, *249*, 810–812, 1974.

NAS/NRC, Causes and effects of stratospheric ozone reduction: An update, National Academy Press, Washington, D.C., 1982.

NASA/JPL, Chemical kinetics and photochemical data for use in stratospheric modeling, Evaluation number 4, NASA Panel for Data Evaluation, *JPL Publ. 81-3*, Jet Propul. Lab., Pasadena, Calif., 1981.

NASA/JPL, Chemical kinetics and photochemical data for use in stratospheric modeling, Evaluation number 5, NASA Panel for Data Evaluation, *JPL Publ. 82-57*, Jet. Propul. Lab., Pasadena, Calif., 1982.

Nicolet, M., Photodissociation of nitric oxide in the mesosphere and stratosphere: Simplified numerical relations for atmospheric model calculations, *Geophys. Res. Lett.*, *6*, 866–868, 1979.

Owens, A. J., J. M. Steed, D. L. Filkin, C. Miller, and J. P. Jesson, The potential effects of increased methane to atmospheric ozone, *Geophys. Res. Lett.*, *9*, 1105–1108, 1982.

Prinn, R. G., F. N. Alyea, and D. M. Cunnold, Photochemistry and dynamics of the ozone layer, *Ann. Rev. Earth Planet. Sci.*, *6*, 43–74, 1978.

Ramanathan, V., and R. E. Dickinson, The role of stratospheric ozone in the zonal and seasonal radiative energy balance of the earth-troposphere system, *J. Atmos. Sci.*, *36*, 1084–1104, 1979.

Rasmussen, R. A., and M. A. K. Khalil, Increase in the concentration of atmospheric methane, *Atmos. Environ.*, *15*, 883–886, 1981.

Smith, C., L. T. Molina, J. Lamb, and M. J. Molina, Kinetics of the reaction of OH radicals with pernitric acid, paper presented at 183rd National Meeting, Am. Chem. Soc., Las Vegas, March 28–April 2, 1982.

Sridharan, W. C., L. X. Qiu, and F. Kaufman, Kinetics and product channels of the reactions of HO_2 with O and H atoms at 296 K, *J. Phys. Chem.*, *86*, 4569–4574, 1982.

Sun, H., and G. L. Weissler, Absorption cross sections of methane and ammonia in the vacuum ultraviolet, *J. Chem. Phys.*, *23*, 1160–1164, 1955.

Turco, R. P., and R. C. Whitten, A note on the diurnal averaging of aeronomical models, *J. Atmos. Terr. Phys.*, *40*, 13–20, 1978.

Weiss, R. F., The temporal and spatial distribution of tropospheric nitrous oxide, *J. Geophys. Res.*, *86*, 7185–7195, 1981.

Wine, P. H., A. R. Ravishankara, N. M. Kreutter, R. C. Shah, J. M. Nicovich, R. L. Thompson, and D. J. Wuebbles, Rate of reaction of OH with HNO_3, *J. Geophys. Res.*, *86*, 1105–1112, 1981.

WMO, *The Stratosphere 1981: Theory and Measurements*, Rep. 11, WMO Global Ozone Res. and Monitering Proj., Geneva, 1982.

Wuebbles, D. J., Chlorocarbon emission scenarios: Potential impact on stratospheric ozone, *J. Geophys. Res.*, *88*, 1433, 1983.

Wuebbles, D. J., and J. S. Chang, A study of the effectiveness of the Cl*X* catalytic ozone loss mechanisms, *J. Geophys. Res.*, *86*, 9869–9872, 1981.

Wuebbles, D. J., F. M. Luther, and J. E. Penner, Effect of coupled anthropogenic perturbations on stratospheric ozone, *J. Geophys. Res.*, *88*, 1444, 1983.

Yao, F., I. Wilson, and H. S. Johnston, Temperature-dependent ultraviolet absorption spectrum for N_2O_5, *J. Phys. Chem.*, *86*, 3611–3615, 1982.

(Received October 13, 1982;
revised December 30, 1982;
accepted January 7, 1983.)